ORIGINAL PAPER

Computational simulations of structural role of the active-site W374C mutation of acetyl-coenzyme-A carboxylase: Multi-drug resistance mechanism

Xiao-Lei Zhu · Wen-Chao Yang · Ning-Xi Yu · Sheng-Gang Yang · Guang-Fu Yang

Abstract Herbicides targeting grass plastidic acetyl-CoA carboxylase (ACCase, EC 6.4.1.2) are selectively effective against graminicides. The intensive worldwide use of this herbicide family has selected for resistance genes in a number of grass weed species. Recently, the active-site W374C mutation was found to confer multi-drug resistance toward haloxyfop (HF), fenoxaprop (FR), Diclofop (DF), and clodinafop (CF) in *A. myosuroides*. In order to uncover the resistance mechanism due to W374C mutation, the binding of above-mentioned four herbicides to both wild-type and the mutant-type ACCase was investigated in the current work by molecular docking and molecular dynamics (MD) simulations. The binding free energies were calculated by molecular mechanics-Poisson-Boltzmann surface area (MM/PBSA) method. The calculated binding free energy values for four herbicides were qualitatively consistent with the experimental order of IC_{50} values. All the computational model and energetic results indicated that the W374C mutation has great effects on the conformational change of the binding pocket and the ligand-protein interactions. The most significant conformational change was found to be associated with the aromatic amino acid residues, such as Phe377, Tyr161′ and Trp346. As a result, the π-π interaction between the ligand and the residue of Phe377 and Tyr161′, which make important contributions to the binding affinity, was decreased after mutation and the binding affinity for the inhibitors to the mutant-type ACCase was less than that to the wild-type enzyme, which accounts for the molecular basis of herbicidal resistance. The structural role and mechanistic insights obtained from computational simulations will provide a new starting point for the rational design of novel inhibitors to overcome drug resistance associated with W374C mutation.

Keywords Acetyl-CoA carboxylase · Computational simulations · π-π Interaction · Resistance mechanism

X.-L. Zhu · W.-C. Yang · N.-X. Yu · S.-G. Yang · G.-F. Yang (✉)
Key Laboratory of Pesticide & Chemical Biology, Ministry of Education, College of Chemistry,
Central China Normal University,
Wuhan 430079, People's Republic of China
e-mail: gfyang@mail.ccnu.edu.cn

Introduction

Acetyl-coenzyme-A carboxylase (ACCase, EC 6.4.1.2) is the rate-limiting enzyme in the *de novo* fatty acid biosynthetic pathway responsible for the conversion of acetyl-CoA to malonyl-CoA. This is a two-step, reversible reaction, consisting of the ATP-dependent carboxylation of the biotin group on the carboxyl carrier domain catalyzed by the biotin-carboxylase and the transfer of the carboxyl group from biotin to acetyl-CoA catalyzed by the carboxyl-transferase (CT) domain [1–3]. In plants, there are two isoforms of ACCase: the plastid ACCase is essential in biosynthesis of primary fatty acids and the cytosolic ACCase is involved in biosynthesis of long chain fatty acids. Inhibitors of this enzyme do more than merely block the production of malonyl-CoA, thus causing plant death [4, 5].

Three chemically dissimilar classes of herbicides that are known to inhibit ACCase are aryloxyphenoxypropionates (APPs), cyclohexanediones (CHDs) and the more recent phenylpyrazolin class herbicide pinoxaden [6–8]. Molecular and biochemical studies have clearly established that the CT domain is the primary target site for APPs, CHDs, and pinoxaden herbicides [9]. The basis of selectivity for these herbicides lies in the structure of the plastid ACCase. Since

their introduction to world agriculture in the 1980s, APPs and CHDs have been widely used to control a number of grass weed species [10]. As a consequence, they rapidly selected, and are still selecting, resistant plants within grass weed species. Thirty-five resistant weed species in 26 countries have been reported so far (see the website of herbicidal resistance at www.weedscience.org/In.asp), which represent a major problem for sustainable agriculture. In most cases, resistance is due to mutation of the ACCase CT domain, making it less sensitive to herbicide inhibition [9–12]. Five amino acid substitutions in the CT domain have been implicated in resistance to APPs and/or CHDs herbicides, including Ile-1781-Leu, Trp-2027-Cys, Ile-2041-Asn, Asp-2078-Gly, and Gly-2096-Ala (numbered according to the *Alopecurus myosuroides* plastid ACCase) [10, 11].

Recently, we have examined the interactions mechanism between wild-type and mutant ACCase and clodinafop (CF) [13]. Mutations of W374C, I388N, D425G, and G443A (alleles to Trp-2027-Cys, Ile-2041-Asn, Asp-2078-Gly, and Gly-2096-Ala) in *A. myosuroides* CT domain would interfere with the π-π interaction and the H-bond interactions between CF and protein. Although our study has indicated clearly that the residue W374 did not directly form interactions with APPs herbicides, the W374C mutation in *A. myosuroides* conferred resistance to APPs but no resistance to CHDs [10]. Most interestingly, W374C mutation showed a different level of resistance to various APPs herbicides with very small structural differences. Therefore, as a continuation of our research work on drug resistance mechanism [13, 14], we were motivated to investigate the detailed resistance mechanism due to the W374C mutation in the *A. myosuroides* CT domain and to evaluate its biological effects by using computational modeling techniques.

In this paper, various computational techniques, including molecular docking, molecular dynamics (MD), and the molecular mechanics-Poisson-Boltzmann surface area calculations (MM/PBSA), were used to uncover the detailed mechanism of the multi-drug resistance due to W374C mutation. Four commercial APPs herbicides, such as haloxyfop (HF), fenoxaprop (FR), Diclofop (DF), and clodinafop (CF) (depicted in Fig. 1) were considered as typical examples in the present study. The computational results revealed that the conformational change of the binding pocket and the decrease in van der Waals interaction caused by the W374C mutation are responsible for the decreased ligand-binding affinity.

Materials and methods

Initial structures

The MD-equilibrated structures for wild-type (WT) *A. myosuroides* CT domain complex with haloxyfop (AM-HF)

and clodinafop (AM-CF) were from our previous work [13]. The initial structures of FR and DF complexed with the wild-type *A. myosuroides* CT domain (AM-FR and AM-DF) were obtained by modifying the structure of HF in the structure of the AM-HF complex. This method has been used in our previous study [13] and in other investigations [15–17]. Then, the process of changing Trp374 to Cys374 was accomplished using the SYBYL molecular simulation package [18] to obtain four mutant-type (MT) complexes. A total of six systems, including two wild-type complexes and four mutant-type complexes, were simulated here.

Molecular dynamics (MD) simulations

The procedures for conducting molecular dynamics simulations for two wild-type complexes (AM-FR and AM-DF) and four mutant-type complexes are similar to our previous studies [13, 19, 20]. There are two symmetric binding pockets in the 3D structure of each complex. Here, to conserve computation costs, we subjected only one binding pocket (including residues from 239 to 546 in one monomer and 1′ to 237′ in the other monomer) to MD simulations.

Standard AMBER force field (ff99) [21, 22] was used for amino acid residues and General AMBER force field (gaff) [23, 24] was used for the ligands. Geometry optimization for each ligand was performed and electrostatic potential was calculated at the HF/6-31G (d) level using the Gaussian 03 program [25]. Atomic charges of the inhibitors were calculated by RESP fitting method. [26] Partial atomic charge and force-field parameters for the inhibitors were generated by the Antechamber suite. All systems were solvated by a 50 Å cap of TIP3P [27] water centered on the inhibitor and then neutralized by added Na^+ ions.

Energy minimizations and MD simulations were carried out using the Sander module of the AMBER 8 package [22]. In the energy minimization and the MD simulation, particle mesh Ewald (PME) was employed to treat the long-range electrostatic interactions [28, 29]. The energy minimization was achieved in two stages. First, the protein was fixed with a constraint of 500 kcal mol^{-1} Å^{-2} and only the positions of water molecules and Na^+ ions were minimized for 3000 steps. Then, the entire system was subjected to 500 step steepest descent (SD) minimization and 5500 steps of conjugate gradient (CG) minimization. The SHAKE algorithm was used to constrain all covalent bonds involving hydrogen atoms, and the time step for MD simulation was set to 2.0 fs. The cutoff distances for the long-range electrostatic and the van der Waals energy terms were set at 10.0 Å. After full relaxation and after the entire solvated system was subjected to further energy-minimization, the system was slowly heated from T=10 K
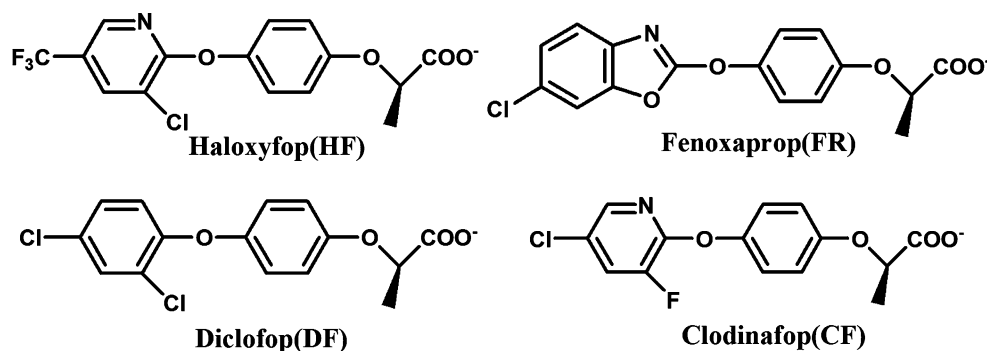
to T=300 K in 30 ps. Meanwhile, additional 30 ps MD simulations at 300 K were carried out with restriction and the equilibrating calculation was executed at pressure of 1 atm and temperature of 300 K. In order to avoid the two monomers appearing in translation, a 100 kcal mol^{-1} Å^{-2} harmonic force constant was set for both monomers of the protein and inhibitor before equilibration simulations. During the MD simulation process, coordinates were collected every 1 ps for the complexes. For each MD-simulated complex, 100 snapshots of the structure simulated in the last 100 ps of the stable MD trajectory were used for calculation of the free energy of binding below.

Binding free energy calculation (MM/PBSA)

The molecular mechanics-Poisson-Boltzmann surface area (MM/PBSA) [30, 31] method was used to calculate the binding free energy. In general, the binding free energy of a protein-ligand complex (ΔG_{bind}) is defined as:

$$\Delta G_{bind} = G_{cpx} - \left(G_{rec} + G_{lig} \right) \qquad (1)$$

where G_{cpx}, G_{rec}, and G_{lig} are the free energies of the receptor/protein-ligand complex, the unoccupied receptor/protein and the free ligand, respectively.

The binding free energy (ΔG_{bind}) can be estimated in terms of the molecular mechanical (MM) gas-phase binding energy (ΔE_{MM}), the solvation free energy (ΔG_{sol}), and the entropic contribution (-TΔS):

$$\Delta G_{bind} = \Delta E_{bind} - T\Delta S \qquad (2)$$

$$\Delta E_{bind} = \Delta E_{MM} + \Delta G_{sol} \qquad (3)$$

ΔE_{MM} was calculated by using the following equation:

$$\Delta E_{MM} = \Delta E_{ele} + \Delta E_{vdw}, \qquad (4)$$

where ΔE_{ele} and ΔE_{vdw} are electrostatic and van der Waals interaction energies, respectively, between a ligand and a protein, computed using the same parameter set as that used in the MD simulation. The solvation free energy ΔG_{sol} is composed of two parts [32, 33]:

$$\Delta G_{sol} = \Delta G_{PB} + \Delta G_{np}. \qquad (5)$$

The electrostatic contribution to the solvation free energy (ΔG_{PB}) can be obtained by solving Poisson-Boltzmann (PB) equation [33]. ΔG_{np} is the nonelectrostatic contribution to the solvation free energy, determined as a function of the solvent accessible surface area (SASA) [32]. Therefore, ΔG_{np} was estimated using a simple empirical relation of $\Delta G_{\text{np}} = \gamma$ SA + b (γ=0.00542 kcal mol^{-1} Å^{-2}, b= 0.92 kcal mol^{-1}), where SASA is determined with the LCPO method as implemented in AMBER 8.0. The interior and exterior dielectric constants were set to 1 and 80, respectively. The grid spacing was set to 2/3 Å. In the first protocol, the structures of protein, ligand, and their complex were taken from the same MD trajectory, stripped of all water molecules and Na^{+} ions. Then, all energy components and binding free energy values were calculated for all three molecules generated from the 100 snapshots. For wild-type and mutant complexes, the intervals were set to 1 ps during the last 100 ps simulations.

Further, the entropic contribution to the binding free energy can be divided into two parts: the solvation entropy change (ΔS_{sol}) and the conformational entropy change (ΔS_{conf}). The detailed computational procedure used to evaluate the entropic contribution (-TΔS) to the binding free energy was the same as that described in our recent publications [13, 14, 34, 35].

Results and discussion

Structures of the wild-type complexes

To explore the dynamic stabilities of four wild-type protein-inhibitor complexes, root-mean-square-displacement (RMSD) values for the protein backbone atoms and the heavy atoms of inhibitor during the production phase relative to the starting structures were determined as shown in Fig. 2. In order to compare the structure characteristics, the results of AM-HF and AM-CF complexes obtained from our previous study [13] were put together herein. The

Fig. 2 Plots of the RMSDs of wild-type *A. myosuroides* CT domain complexed with HF (**a**), FR (**b**), DF (**c**), CF (**d**). The black line represents the RMSD of backbond atoms of receptor except the end terminal of each monomer (the residues 57–122, 448–516, 56′–124′ and 453′–516′) and red line represents the RMSD of heavy atoms in each ligand
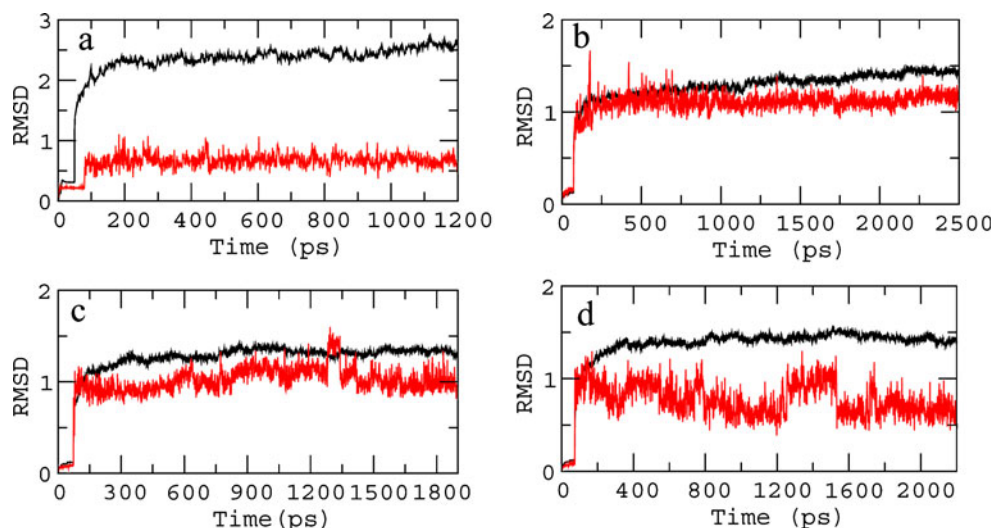
RMSD plots indicated that the four wild-type complexes achieved equilibrium very quickly. We also examined the dihedral angle changes of the inhibitor in AM-HF, AM-FR, AM-DF, and AM-CF complexes (as shown in Fig. 1s in supporting information) and the distance changes between the centroid of the aromatic rings of four inhibitors (the pyridyl ring of HF and CF, benzene ring of DF, and benzoxazol ring of FR) and the phenyl ring of Phe377 and Tyr161′ which formed π-π interactions with the inhibitor (as shown in Fig. 2s in supporting information). All these data confirmed that the four wild-type complexes have achieved equilibrium after MD simulations. The averaged structure after MD simulation of AM-HF, AM-FR, AM-DF, and AM-CF showed that the binding models for HF, FR, DF, and CF with wild-type *A. myosuroides* CT domain were similar as shown in Fig. 3. In AM-HF (Fig. 3a) complex, the pyridyl ring of HF was sandwiched by Phe377 and Tyr161′ (allele to Phe1956′ and Tyr1738 in the crystal structure of *yeast* CT domain in complex with HF, as shown in Fig. 4) via π-π interactions. The carboxyl oxygen atoms of HF formed a H-bond interaction with Ile158′ (allele to Ile1735 in the complex crystal structure). This MD-simulated binding model is similar to that of HF in the crystal structure of the complex [5]. Considering the AM-DF (Fig. 3c) and AM-CF (Fig. 3d) complexes, both the benzene ring of DF and the pyridyl ring of CF formed a sandwich π-π interaction with the residues Phe377 and Tyr161′ and the carboxyl oxygen atoms of DF and CF formed H-bonds with the residues Ile158′ and Ala54′. An interesting phenomenon was observed for the AM-FR complex. As shown in Fig. 3b, the benzoxazol ring of FR was not only sandwiched between Phe377 and Tyr161′ *via* π-π interactions but also showed a π-π interaction with Trp346, which could account for its superior IC_{50} value. At the same time, the carboxyl oxygen atoms of FR formed H-bonds with Ile158′ and Ala54′. Therefore, the primary interaction between the four APPs herbicides and the wild-type CT domain appear to be π-π interactions and H-bond interactions.

In addition, we also calculated the binding free energies for four APPs herbicides using the MM/PBSA method (Table 1). According to the energy components of the binding free energies (Table 1), the major favorable contributions to ligand binding are the van der Waals and polar solvation terms. The non-polar solvation term, which corresponds to the burial of SASA upon ligand binding, contributes slightly favorably. The order of calculated binding free energies (ΔG_{bind}) is FR>HF> DF> CF and corresponds qualitatively with the order of the experimentally determined IC_{50} values (Table 1). Thus, the binding model for APPs herbicides after MD simulations should be reasonable. These simulated binding models are the basis for the following herbicide resistance mechanism study.

Comparison of the structures of wild-type and W374C models

The starting structures of the four W374C mutant complexes were obtained by direct substitution of the residue from Trp374 to Cys374 and then these structures were subjected to MD simulations (Fig. 3s in the supporting information). To investigate the influence of the W374C mutation on the conformations of the binding pocket, the averaged structures of the W374C models after MD simulation were superimposed on those of the corresponding wild-type complexes as shown Fig. 3. The results indicated that residues Trp346, Phe377, and Tyr161′ in these complexes always underwent significant conformational changes after W374C mutation, which resulted in the decrease of the π-π interaction energy between the protein and inhibitors (Fig. 5).
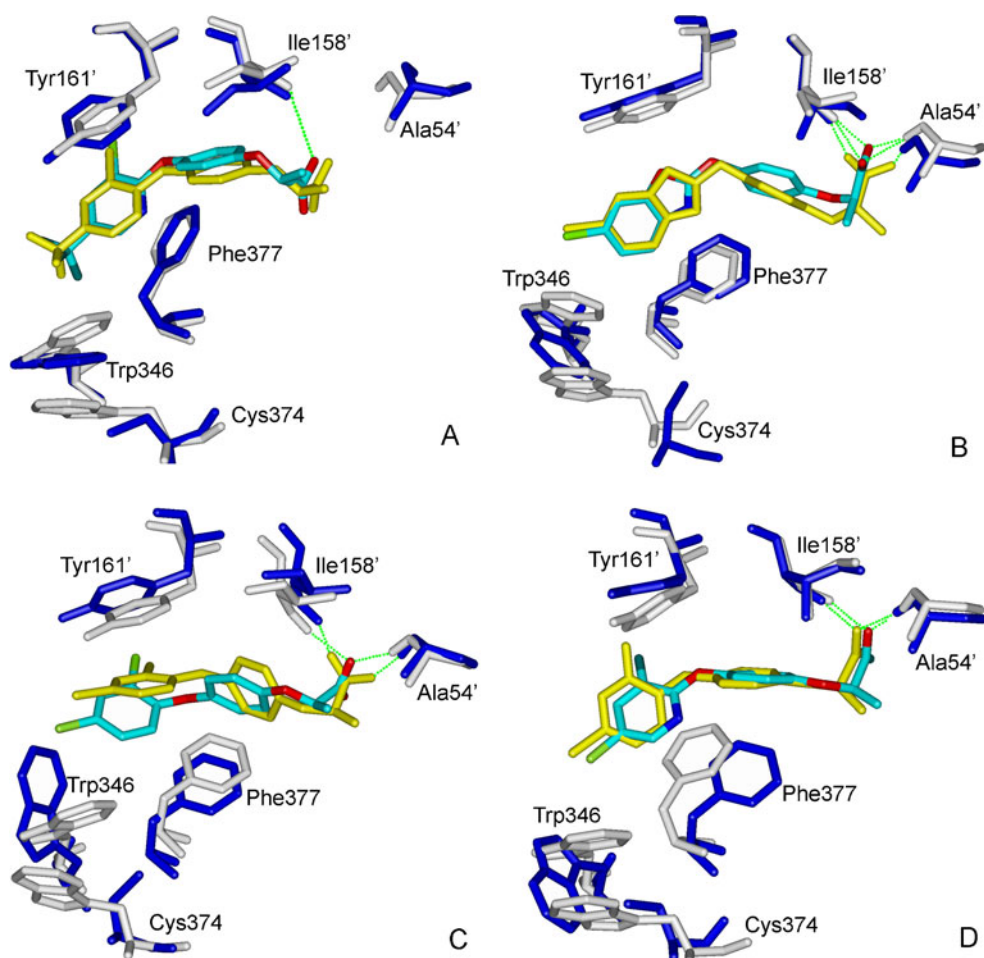
Fig. 3 The overlay between the structure of wile-type AM-HF (**a**), AM-FR (**b**), AM-DF (**c**), and AM-CF (**d**) and its corresponding W374C mutant complex. Wide-type complex was colored by gray and cyan. W374C mutant complex was colored by blue and yellow

To identify the detailed effects of the site mutation on the contribution of structural units of these inhibitors to the binding energy, the inhibitor was split into three subunits (sub_1, sub_2, and sub_3) and then we calculated the binding energy for each subunit with the protein using the MM/PBSA method. As shown in Table 2, the introduction of the W374C mutation decreased the binding energies (ΔE_{bind}) for all three subunits of FR, DF and CF. As a result, these three herbicides showed significant resistance upon W374C mutation. In addition, based on the ΔE_{bind} values as shown in Table 2, the binding energies (ΔE_{bind}) for the HF subunits were ranked in the order sub_1> sub_2> sub_3. Although sub_1 of the HF inhibitor appears to make the most favorable contribution to ligand binding in the complex with wild-type ACCase CT domain, it suffered energy lost of 1.66 kcal mol^{-1} after W374C mutation. However, sub_2 and sub_3 got respectively 0.24 kcal mol^{-1} and 1.44 kcal mol^{-1} increase after the mutation, providing a reasonable explanation why compound HF showed the lowest resistance level.
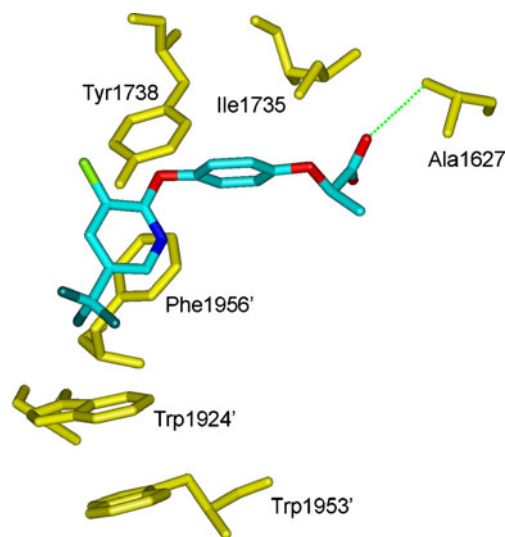

Fig. 4 The binding model HF in the crystal complex (PDB id 1UYS). The residues of Trp1953′, Trp1924′, Phe1956′, Tyr1738′, Ile1735′, and Ala1627 allele to Trp374, Trp346, Phe377, Tyr161′, Ile158′, and Ala54′, respectively

Table 1 Binding free energies (kcal mol^{-1}) of HF, FR, DF, and CF complexed with wild-type or the mutant-type protein

ligand	protein	ΔE_{ele}	ΔE_{VDW}	ΔE_{np}	ΔE_{polar}	ΔE_{bind}	-TΔS	ΔG_{bind}	$\Delta\Delta G_{bind}$[a]	IC$_{50}$ (uM)	RF[b]	$\Delta\Delta G_{exp}$[c]
HF	WT	68.80	-43.70	-4.93	-42.20	-22.03	6.81	-15.22		1.4	—	—
	W374C	65.37	-41.74	-5.02	-40.33	-21.71	8.21	-13.50	1.72	26.6	19	0.32
FR	WT	38.72	-46.47	-5.10	-11.33	-24.17	7.57	-16.60		0.7	—	—
	W374C	55.36	-43.63	-5.27	-25.95	-19.49	8.17	-11.32	5.28	37.0	53	0.74
DF	WT	51.51	-45.08	-4.98	-23.51	-22.06	8.48	-13.58		2.2	—	—
	W374C	56.00	-42.48	-5.03	-25.70	-17.20	5.89	-11.31	2.27	21.5	21.5	0.49
CF	WT	46.30	-40.71	-4.96	-20.75	-20.13	7.87	-12.26		4.0	—	—
	W374C	42.22	-41.61	-4.87	-8.50	-12.76	9.24	-3.52	8.74	361.8	90.5	1.29

[a] $\Delta\Delta G_{bind} = \Delta G_{MT} - \Delta G_{WT}$

[b] RF = IC$_{50, MT}$/IC$_{50, WT}$, IC$_{50}$ values were taken from Ref. 10

[c] $\Delta\Delta G_{exp} = RT\ln(IC_{50, MT}$/IC$_{50, WT}) = 1.366\log$RF

We previously reported the conformational changes that occurred at the same residues[13]. However, there are small differences between the results of the present study and those of the previous study regarding the residues at the binding pocket. In the case of mutant-type AM-HF, as shown in Fig. 3a, there is an important π-π interaction between the side indole rings of Trp346 and Trp374 in the wild-type complex, which disappeared after the W374C mutation. As a result, the indole ring of Trp346 and the benzene ring of Tyr161′ rotated about 40° and 10° upon mutation, respectively. Meanwhile, the centroid of the benzene ring of Phe377 translated toward the right by ~0.67 Å. Considering the mutant-type AM-FR complex (Fig. 3b), the indole ring of Trp346 rotated ~50° and then the centroid of Trp346 translated toward left ~2.43 Å upon mutation. At the same time, the centroid of Tyr161′ and Phe377 translated toward the right and downward ~1.37 Å and 1.41 Å, respectively. Analyzing mutant-type AM-DF complex (Fig. 3c), the indole ring of Trp346 and the

benzene ring of Tyr161′ rotated ~80° and 30° upon mutation, respectively. Meanwhile the centroid of Phe377 and Tyr161′ translated upward ~0.99 Å and toward the left by 0.85 Å. For mutant-type AM-CF complex (Fig. 3d), the indole ring of Trp346 and the benzene ring of Tyr161′ rotated ~60° and 20° upon mutation, respectively. The centroid of Phe377 translated toward the right by ~2.70 Å. Interestingly, the conformation of the bound HF, FR, and CF inhibitors were relatively conserved upon binding to the W374C variant. In contrast, bound DF underwent significant conformational change in the binding site of after mutation, which might account for its lower resistance relative to FR and CF.

Binding free energies and drug resistance

The influence of the W374C mutation on the binding free energy (ΔG_{bind}) was examined for each modeled complex structure. Table 1 compares the binding free energy

Fig. 5 Comparison of the VDW interactions between the inhibitor and some important residues in WT and MT enzyme
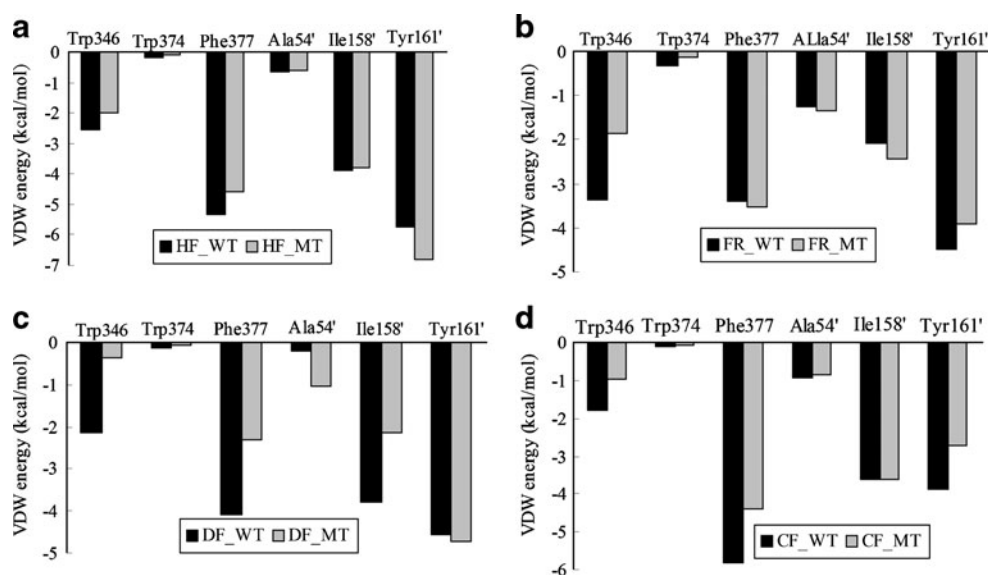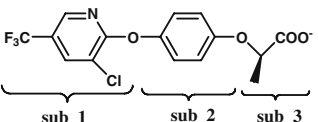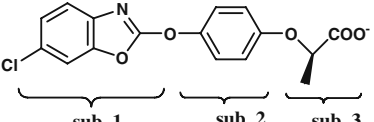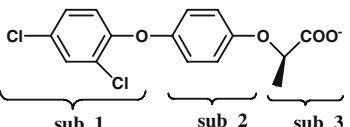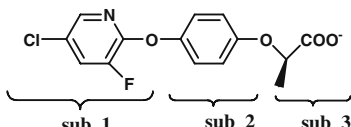
Table 2 The energy (kcal mol^{-1}) contributions of each subunit in HF, FR, DF, and CF

HF	sub_1		sub_2		sub_3		FR	sub_1		sub_2		sub_3	
	WT	MT	WT	MT	WT	MT		WT	MT	WT	MT	WT	MT
ΔE_{ele}	27.73	25.55	6.80	7.58	34.24	32.28	ΔE_{ele}	25.88	27.01	3.59	4.95	9.35	23.41
ΔE_{VDW}	-22.86	-21.91	-12.69	-12.46	-8.16	-7.38	ΔE_{VDW}	-22.33	-23.76	-13.76	-11.19	-10.37	-8.65
ΔE_{np}	-3.31	-3.44	-2.72	-2.74	-2.41	-2.42	ΔE_{np}	-3.23	-3.37	-2.85	-2.78	-2.40	-2.42
ΔE_{polar}	-15.78	-12.76	1.22	-0.01	-27.27	-27.51	ΔE_{polar}	-13.46	-12.31	5.47	2.54	-5.59	-17.00
ΔE_{bind}	-14.22	-12.56	-7.39	-7.63	-3.60	-5.04	ΔE_{bind}	-13.13	-12.42	-7.56	-6.48	-9.00	-4.67

DF	sub_1		sub_2		sub_3		CF	sub_1		sub_2		sub_3	
	WT	MT	WT	MT	WT	MT		WT	MT	WT	MT	WT	MT
ΔE_{ele}	25.85	25.07	6.95	13.94	18.83	16.98	ΔE_{ele}	22.40	22.87	5.63	7.90	18.26	10.41
ΔE_{VDW}	-20.72	-19.33	-14.10	-12.89	-10.29	-10.33	ΔE_{VDW}	-18.87	-18.50	-12.45	-13.68	-9.39	-9.40
ΔE_{np}	-3.12	-3.13	-2.79	-2.80	-2.46	-2.55	ΔE_{np}	-3.09	-2.98	-2.72	-2.75	-2.46	-2.51
ΔE_{polar}	-14.08	-13.71	2.87	-3.39	-10.76	-8.33	ΔE_{polar}	-12.14	-11.06	1.26	3.25	-10.88	-0.61
ΔE_{bind}	-12.06	-11.10	-7.07	-5.11	-4.68	-4.20	ΔE_{bind}	-11.70	-8.66	-8.28	-5.28	-4.47	-2.11

components of all of the ligands in complex with the wild-type and mutant-type *A. myosuroides* CT domain. The binding energy (ΔE_{bind}, neglecting the entropic contribution) calculated for all ligands bound with wild-type protein range from -20.13 to -24.17 kcal mol^{-1}, with FR having the highest ΔE_{bind} value and CF having the lowest. However, the calculated ΔE_{bind} values for the mutant-type protein binding with the ligands ranged from -12.76 to -21.71 kcal mol^{-1}. Compared with the calculated entropic contributions (-TΔS) for the wild type complexes, HF, FR, and CF experienced entropic increases, while DF experienced entropic loss. The Gibbs binding free energies (ΔG_{bind}) calculated for all mutant-type ligand-protein complexes ranged from -3.52 to -13.50 kcal mol^{-1}.

The relative binding free energy shifts ($\Delta\Delta G_{bind}$) from the wild-type to mutant-type protein calculated for the inhibitors can be used to qualitatively predict the resistance levels for the inhibitors due to W374C mutation. According to the calculated $\Delta\Delta G_{bind}$ values (Table 1), the W374C mutation should cause herbicide resistance for all of the inhibitors listed in Table 1 and the highest resistance level should be associated with CF. It is important to compare our computational results with available experimental data. In order to eliminate the experimental error of the reported IC$_{50}$ values, we defined resistance factor (RF =IC$_{50, MT}$/IC$_{50, WT}$) as an index to compare the relative resistance level. Although the experimental IC$_{50}$ values should not be compared quantitatively with the calculated

enzyme-inhibitor binding affinities, it is reasonable to assume that the *RF* are usually (although not generally) consistent with the relative binding free energies ($\Delta\Delta G_{bind}$ =ΔG_{MT} - ΔG_{WT}) of the inhibitor with the wild-type and mutant-type enzyme. As shown in Table 1, the calculated $\Delta\Delta G_{bind}$ values are consistent with the *RF*. In addition, there is a good linear correlation (r^2=0.98) between the calculated $\Delta\Delta G_{bind}$ values and the $\Delta\Delta G_{exp}$ values derived from the experimental resistance data ($\Delta\Delta G_{exp} = RT\ln RF =$ 1.366logRF), suggesting that the herbicide resistance due to the residue mutation is mainly attributed to the decrease in the binding affinity for the inhibitor.

Conclusions

In summary, the mechanism of resistance due to W374C mutation has been uncovered through extensive computational simulations. For the wild-type *A. myosuroides* CT domain, the primary interactions between four APPs herbicides and the protein were π-π interaction and H-bond interaction. Due to the π-π interaction between the side chain of Trp374 and Trp346, the residues of Trp346 could induce Phe377 to adapt such a favorable conformation that Phe377 and Tyr161′ would form a sandwich π-π interaction with the aromatic ring of all the herbicide ligands. The carboxyl oxygens of all ligands form H-bond with the residues of the Ile158′ and/or Ala54′. After W374

mutation, the π-π interaction between the side chain of Cys374 and Trp346 disappeared. As a result, the conformation of Phe377 underwent significant change, decreasing the sandwich π-π interactions between the ligand and the residue of Phe377 and Tyr161′. Therefore, the mutant-type CT has a lower affinity for the inhibitor binding than the wild-type CT, which is the molecular basis of herbicidal resistance. The structural and mechanistic insights obtained from the present study will provide valuable clues for future design of promising compounds to reduce herbicide resistance associated with the W374C mutation.

References

1. Nikolau BJ, Ohlrogge JB, Wurtele ES (2003) Plant biotin-containing carboxylases. Arch Biochem Biophy 414:211–222
2. Egli MA, Gengenbach BG, Gronwald JW, Somers DA, Wyse DL (1993) Characterization of maize acetyl-coenzyme A carboxylase. Plant Physiol 101:499–506
3. Harwood JL (1988) Fatty acid metabolism. Annu Rev Plant Physiol 39:101–138
4. Post-Beittenmiller D (1996) Biochemistry and molecular biology of wax production in plants. Annu Rev Plant Physiol Plant Mol Biol 47:405–430
5. Zhang H, Tweet B, Tong L (2004) Molecular basis for the inhibiton of the carboxyltransferase domain of acetyl coenzyme-A carboxylase by haloxyfop and diclofop. Proc Natl Acad Sci USA 101:5910–5915
6. Hofer U, Muehlebach M, Hole S, Zoschke A (2006) Pinoxaden-for broad spectrum grass weed management in ceral crops. J Plant Dis Prot 20:989–995
7. Rendina AR, Craig-Kennard AC, Beaudoin JD, Breen MK (1990) Inhibition of acetyl-coenzyme A carboxylase by two classes of grass-selective herbicides. J Agric Food Chem 38:1282–1287
8. Burton JD, Gronwald JW, Keith RA, Somers DA, Gegenbach BG, Wyse DL (1991) Kinetics of inhibition of acetyl-coenzyme A carboxylase by sethoxydim and haloxyfop. Pestic Biochem Physiol 39:100–109
9. Yu Q, Collavo C, Zheng MQ, Owen M, Sattin M, Powles S (2007) Diversity of ACCase mutations in resistant Lolium populations: evaluation using clethodim. Plant Physiol 145:547–558
10. Délye C, Zhang XQ, Michel S, Matejicek A, Powles SB (2005) Molecular bases for sensitivity to acetyl-coenzyme a carboxylase inhibitors in black-grass. Plant Physiol 137:794–806
11. Liu WJ, Harrison DK, Chalupska D, Gornicki P, O'Donnell CC, Adkins SW, Haselkorn R, Williams RR (2007) Single-site mutations in the carboxyltransferase domain of plastid acetyl-CoA carboxylase confer resistance to grass-specific herbicides. Proc Natl Acad Sci USA 104:3627–3632
12. Délye C (2005) Weed resistance to acetyl coenzyme A carboxylase inhibitors: an update. Weed Sci 53:728–746
13. Zhu XL, Hao GF, Zhan CG, Yang GF (2009) Computational simulations of the interactions between acetyl-coenzyme-a carboxylase and clodinafop: resistance mechanism due to active and nonactive site mutations. J Chem Inf Model 49:1936–1943
14. Hao GF, Zhu XL, Ji FQ, Zhang L, Yang GF, Zhan CG (2009) Understanding mechanism of drug resistance due to a codon deletion in protoporphrinogen oxidase through computational modeling. J Phys Chem B 113:4865–4875
15. Rafi SB, Cui GL, Song K, Cheng XL, Tonge PJ, Simmerling C (2006) Insight through molecular mechanics poisson−boltzmann surface area calculations into the binding affinity of triclosan and three analogues for fabi, the e. coli enoyl reductase. J Med Chem 49:4574–4580
16. Hou TJ, Yu R (2007) Molecular dynamics and free energy studies on the wild-type and double mutant hiv-1 protease complexed with amprenavir and two amprenavir-related inhibitors: mechanism for binding and drug resistance. J Med Chem 50:1177–1188
17. Weis A, Katebzadeh K, Söderhjelm P, Nilsson I, Ryde U (2006) Ligand affinities predicted with the mm/pbsa method: dependence on the simulation method and the force field. J Med Chem 49:6596–6606
18. SYBYL 7.1, Tripos International, 1699 South Hanley Rd, St Louis, Missouri, 63144, USA
19. Zhu XL, Zhang L, Chen Q, Wan J, Yang GF (2006) Interactions of aryloxyphen- oxypropionic acids with sensitive and resistant acetyl-coenzyme a carboxylase by homology modeling and molecular dynamic simulations. J Chem Inf Model 46:1819–1826
20. Gao DQ, Cho H, Yang WC, Pan YM, Yang GF, Tai HH, Zhan CG (2006) Computational design of a human butyrylcholinesterase mutant for accelerating cocaine hydrolysis based on the transition-state simulation. Angew Chem Int Ed 45:653–657
21. Hornak V, Abel R, Okur A, Strockbine B, Roitberg A, Simmerling C (2006) Comparison of multiple Amber force fields and development of improved protein backbone parameters. Proteins 65:712–725
22. Case, DA, Darden T, Cheatham TE III, Simmerling CL, Wang J, Duke RE, Luo R (2004) AMBER8 users' manual; University of California
23. Case DA, Darden TA, Cheatham TE III, Simmerling CL, Wang J, Duke RE, Luo R, Merz KM, Wang B, Pearlman J, Hornak V, Cui G, Beroza P, Schafmeister C, Caldwell JW, Rose WS, Kollman PA (2004) AMBER8. University of California, San Francisco, CA
24. Wang J, Wolf RM, Caldwell JW, Kollman PA, Case DA (2004) Development and testing of a general amber force field. J Comput Chem 25:1157–1174
25. Frisch MJ, Trucks GW, Schlegel HB, Scuseria GE, Robb MA, Cheeseman JR, Montgomery JA Jr, Verven T, Kudin KN, Burant JC, Millam JM, Iyengar SS, Tomasi J, Barone V, Mennucci B, Cossi M, Scalmani G, Rega N, Petersson GA, Nakatsuji H, Hada M, Ehara M, Toyota K, Fukuda R, Hasegawa J, Ishida M, Nakajima T, Honda Y, Kitao O, Nakai H, Klene M, Li X, Knox JE, Hratchian HP, Cross JB, Adamo C, Jaramillo J, Gomperts R, Stratmann RE, Yazyev O, Austin AJ, Cammi R, Pomelli C, Ochterski JW, Ayala PY, Morokumo K, Voth GA, Salvador P, Dannenberg JJ, Zakrzewski VG, Dapprich S, Daniels AD, Strain MC, Farkas O, Malick DK, Rabuck AD, Raghavachari K, Foresman JB, Ortiz JV, Cui Q, Baboul AG, Clifford S, Cioslowski J, Stefanov BB, Liu G, Liashenko A, Piskorz P, Komaromi I, Martin RL, Fox DJ, Keith T, Al-Laham MA, Peng CY, Nanayakkara A, Challacombe M, Gill PM, Wong MW, Gonzalez C, Pople JA (2003) Gaussian 03, Rev A.1. Gaussian Inc, Pittsburgh
26. Cornell WD, Cieplak P, Bayly CI, Kollmann PA (1993) Application of RESP charges to calculate conformational energies, hydrogen bond energies, and free energies of solvation. J Am Chem Soc 115:9620–9631
27. Jorgensen WL, Chandrasekhar J, Madura JD (1983) Comparison of simple potential functions for simulating liquid water. J Chem Phys 79:926–935

28. Darden T, York D, Pedersen L (1993) Particle mesh Ewald: An N·log (N) method for Ewald sums in large systems. J Chem Phys 98:10089–10092
29. Essmann U, Perera L, Berkowitz ML (1995) A smooth particle mesh Ewald method. J Chem Phys 103:8577–8593
30. Srinivasan J, Cheatham TE III, Kollman P, Case DA (1998) Continuum solvent studies of the stability of DNA, RNA, and phosphoramidate-DNA helices. J Am Chem Soc 120:9401–9409
31. Kollman PA, Massova I, Reyes C, Kuhn B, Huo S, Chong L, Lee T, Duan Y, Wang W, Donini O, Ciplak P, Srinivasan J, Case DA, Cheatham TE III (2000) Calculating structures and free energies of complex molecules: combining molecular mechanics and continum models. Acc Chem Res 33:889–897
32. Sitkoff D, Sharp KA, Honig B (1994) Accurate calculation of hydration free energies using macroscopic solvent models. J Phys Chem 98:1978–1988
33. Gilson MK, Sharp KA, Honig BH (1987) Calculating the electrostatic potential of molecules in solution: method and error assessment. J Comput Chem 9:327–335
34. Ji FQ, Niu CW, Chen CN, Chen Q, Yang GF, Xi Z, Zhan CG (2008) Computational design and discovery of conformationally flexible inhibitors of acetohydroxyacid synthase to overcome drug resistance associated with the W586L mutation. Chem Med Chem 3:1203–1206
35. Pan YM, Gao DQ, Zhan CG (2008) Modeling the catalysis of anti-cocaine catalytic antibody: competing reaction pathways and free energy barriers. J Am Chem Soc 130:5140–5149